JOURNAL OF Applied Polymer SCIENCE

High Temperature Ablation of Highly Filled Polymer-Layered Silicate Nanocomposites

Azin Paydayesh, Mehrdad Kokabi, Ahmad Reza Bahramian
Polymer Engineering Department, Faculty of Chemical Engineering, Tarbiat Modares University, P.O. Box 14115-114, Tehran, Islamic Republic of Iran
Correspondence to: M. Kokabi (E-mail: mehrir@modares.ac.ir)

ABSTRACT: At instantaneous thermal shocks and high temperature conditions, using the charring ablative heat shields is more effective than the other heat protection methods. In recent years, low-filled layered silicate polymeric nanocomposites were introduced as new class of ablative materials. In this work, highly filled ablative polymeric nanocomposite is prepared and its thermal stability and ablation mechanism is studied under high external heat flux. The thermal degradation kinetics during pyrolysis, the variation of thermophysical properties as a result of ablation process and mathematical modeling of ablation process are performed for highly filled ablative polymeric nanocomposite samples compared with those of their composite counterparts under oxyacetylene flame test. The results show that the ablation performance of highly filled polymeric nanocomposite is higher than that of the composite, and the mathematical model is adequately confirmed by the experimental data of the thermophysical and ablation properties of highly filled nanocomposites. © 2012 Wiley Periodicals, Inc. J. Appl. Polym. Sci. 000: 000–000, 2012

KEYWORDS: composites; thermal properties; highly filled nanocomposite; pyrolysis; resole resin

Received 6 June 2011; accepted 28 February 2012; published online
DOI: 10.1002/app.37588

INTRODUCTION

Ablation is a geological term of at least 120 years old and generally named for surface mass removal from a body as a result of thermochemical and mechanical processes.[1,2] In aerospace technology, ablation is a self-regulation heat and mass transfer process for thermal protection because heat shields against the external enormous temperature loaded on the re-entry vehicles when arrived into the earth's atmosphere.[3,4]

An ablative material, in a sacrificial way, absorbs heat as a result of physical and chemical changes to save substrate and finally consume it.[5] Ablation is an order of heat and mass transfer process in which a large amount of thermal energy is expended by sacrificial loss of surface region material.[6–11] The heat input from the environment is absorbed, blocked, dissipated, and generated by numerous mechanisms. They involve (1) heat conduction into the material substrate and storage by its effective heat capacity, (2) materials phase changes such as melting, vaporization, and sublimation, (3) heat absorption by gases in the substrate as they percolate to the surface, (4) convection of heat in a liquid layer, if exists one, (5) transpiration of gases from the ablating surface into the boundary layer with attendant heat absorption, (6) surface and bulk radiation, (7) endothermic and exothermic chemical reactions, and (8) possible yet unrecognized reactions. Such energy absorptive processes take place automatically, simultaneously control the surface temperature, and greatly restrict the inward flow of heat. The characteristics of ablative thermal protection materials are illustrated in Figure 1.

Charring ablators are the most widely used thermal protection shield because of producing a char insulation layer on the surface.[3,6] This surface layer plays a predominant role in the absorption of heat by endothermic processes and thus increases the performance of ablative insulators, moreover does not reduce their volume significantly. In fact, the presence of char layer regulates penetration of heat from the surface and produces a steep temperature gradient.[12–15]

Ablation behavior of materials depends mainly on their intrinsic properties. Because of having some properties such as excellent ablation resistance, high char yielding, and good mechanical properties, use of phenolic matrix composites is the best choice as ablative heat shields.[16–18] Despite wide usage of polymeric composites ablators, their performance is limited due to mechanical weakness of resulting char that makes insulator susceptive to mechanical erosion. This weakness reduces strongly the lifetime of insulation and necessitates additional thickness.[4]

Applied Polymer SCIENCE

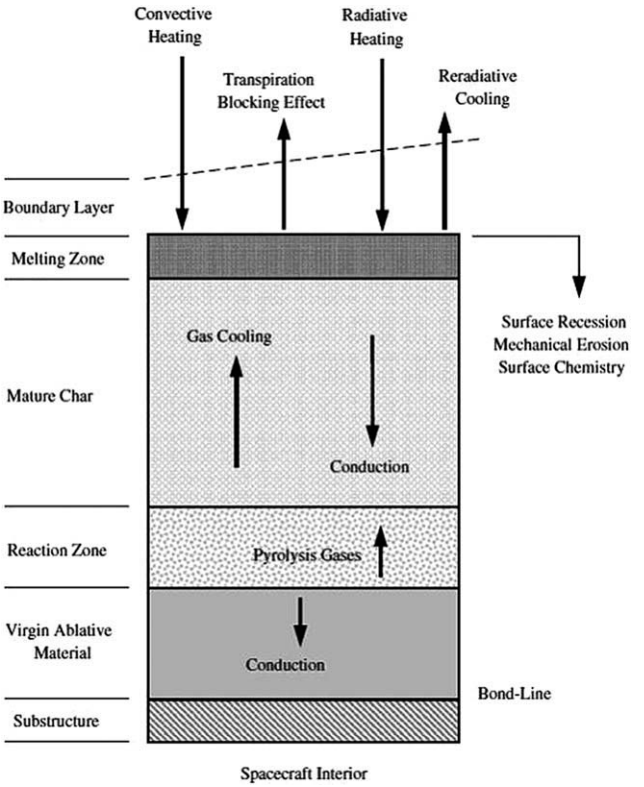

Figure 1. Schematics of the charring ablation phenomenon.

In recent years, the polymeric-layered silicate nanocomposites were investigated as a new class of ablative materials by Vaia et al.,[4] Koo et al.,[19,20] and Bahramian et al.[21,22] Also Natali et al. prepared and optimized the production technique of the phenolic-layered silicate nanocomposites for ablation applications. Although they did not carry out any ablation tests, they obtained a good degree of dispersion and a uniform distribution of the nanoclay platelets in phenolic matrix. The produced nanocomposite was suggested as a potential ablative material.[23]

The results show good ablation performance for nanocomposite systems compared with traditional composites. These nanocomposite systems exhibit such behavior because on pyrolysis, a uniform ceramic char forms on the ablated surface which may lead to significantly increase oxidation and mechanical erosion resistance.

High effective ceramic char layer of nanocomposite encourages us to examine the highly filled polymeric nanocomposite systems as ablative heat shields. Attention to highly filled polymeric nanocomposite that consists of high amount of layered silicate in contrast to traditional nanocomposites in which the clay loading level is about 1-7 wt % is a new idea in nanocomposites field that has been reported only by few researchers.[24–28]

In this work, a comparative study of ablation performance of highly filled phenolic/asbestos/montmorillonite nanocomposite was conducted against its composite counterpart. The heat diffusion through the thickness and erosion rate was measured for both systems. Ablation mechanism, thermal degradation kinetics, and thermophysical properties of highly filled ablative nanocomposites were also investigated. Finally, the mathematical model was evaluated by the experimental data.

It is worth bearing in mind that albeit asbestos fibers have unique thermal properties for this special application; also significant exposure to asbestos increases the risk of developing lung disease, and that risk is made worse by smoking. When asbestos fibers are inhaled, most fibers are expelled, but some can become lodged in the lungs and remain there throughout the life.

Table I. Properties of Resole Type Phenolic Resin

Property	Value
Density (kg m^{-3})	1050
Viscosity of liquid resin at 20°C (Pa s)	5.5-6.5
Solid content (wt %)	87
Specific heat (J kg^{-1} K^{-1})	2000
Thermal conductivity (J m^{-1} s^{-1} K^{-1})	0.35
Gasification coefficient	0.6

Table II. Properties of Asbestos Cloth

Property	Value
Density (kg m^{-3})	2000
Specific heat (J kg^{-1} K^{-1})	787
Thermal conductivity (J m^{-1} s^{-1} K^{-1})	0.65
Maximum moisture (wt %)	2.5
Minimum asbestos (wt %)	90
Maximum mass loss at 820°C (wt %)	23
Weave	Plain
Thickness (mm)	2

Ablation Mathematical Model

Under the experimental conditions (oxyacetylene flame test), complex processes of heat and mass transfer are taken place in polymeric heat shields. During the experimental conditions, heat shields are exposed to high temperature and high velocity fluid stream. At pyrolysis temperature, resin begins to decompose and char layer ablation is created at higher temperatures. The free surface of the heat shields under the influence of high temperature gas stream is continuously spilled and oxidized depending on the oxygen content in the gases. Therefore, three zones are formed; virgin material, pyrolysis zone, and porous char layer.

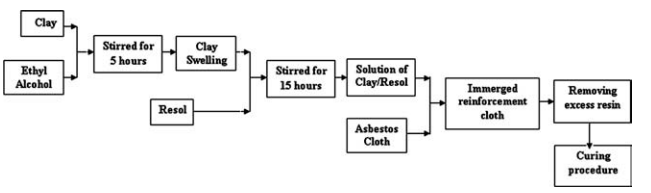

Figure 2. Preparation procedures of the highly filled nanocomposite samples based on phenolic resin.

Table III. Nanocomposites and Composite Samples Compositions and Their Codes

Sample code	Components	Clay content (phr)	Clay (wt %)	PR (wt %)	Asbestos (wt %)
Composite	Asbestos/PR	0	0	50	50
40	Asbestos /PR/MMT	40	14	35	51
50	Asbestos /PR/MMT	50	16	32	52
60	Asbestos /PR/MMT	60	17	29	54
70	Asbestos /PR/MMT	70	18	26	56

PR, phenolic resin; MMT, montmorillonite.

The problem can mathematically be described by the following transient partial differential heat conduction equation, which was introduced in our previous works.[29–31]

$$\rho c\frac{dT}{dt}+\Delta H_p\frac{d\rho}{dt}+c_g m_p\frac{\partial T}{\partial y}=\frac{\partial}{\partial y}\left(K\frac{\partial T}{\partial y}\right), \quad (1)$$

where, ρ, density (kg m^{-3}); c, heat capacity (J kg^{-1} K^{-1}); ΔH_p, heat of ablation (J kg^{-1}); K, thermal conductivity (J m^{-1} s^{-1} K^{-1}); c_g, heat capacity of the gas (J kg^{-1} K^{-1}); and m_p, specific pyrolysis mass flow rate (kg m^{-2} s^{-1}).

The mathematical model illustrates the thermal decomposition, thermophysical properties, and ablation. The main assumptions on which the model rests were mentioned in our last publications.[22,30,31] Therefore, in here, we are not going to repeat the details of the mathematical model but willing to evaluate the model by the experimental data.

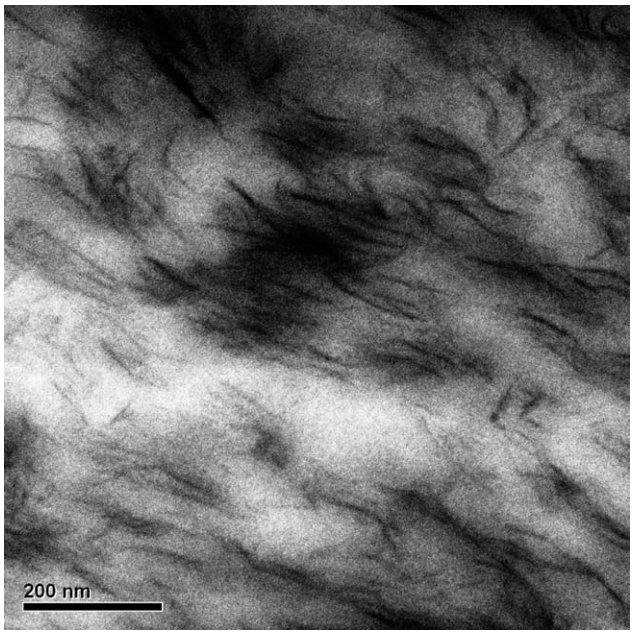

Figure 3. TEM image of a typical nanocomposite containing 50 phr organoclay in the absence of asbestos fibers.

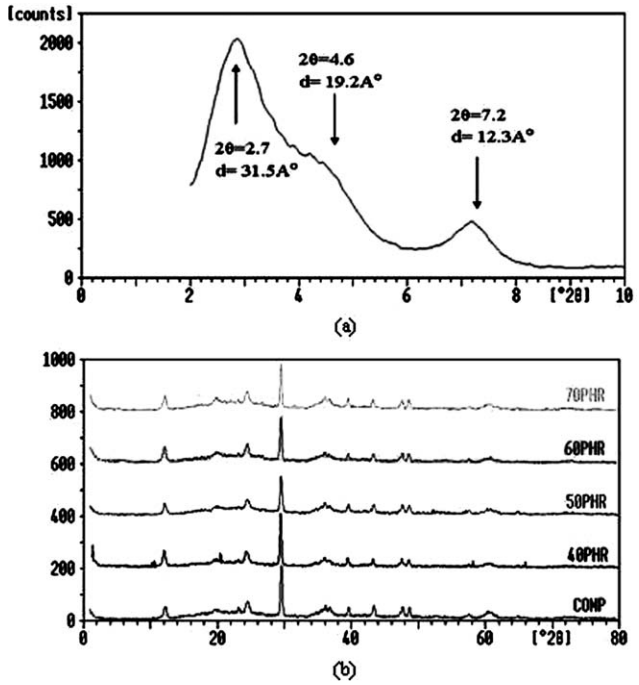

Figure 4. XRD patterns of (a) cloisite 15A and (b) phenolic nanocomposites.

EXPERIMENTAL

Materials

A resole type phenolic resin (IL800/2) supplied by Resitan Co., Iran, with the properties given in Table I was used as the polymeric matrix. Asbestos cloth (Grade AAA) was added as reinforcing to the phenolic resin matrix which properties are given in Table II. The modified montmorillonite (Cloisite 15A) as nanofillers used in this work was obtained from Southern Clay Products, USA.

Sample Preparation

For preparation of the composite samples, asbestos cloth was properly impregnated by phenolic resin. The fiber/resin ratio was adjusted to 50/50 wt %. To prepare the highly filled

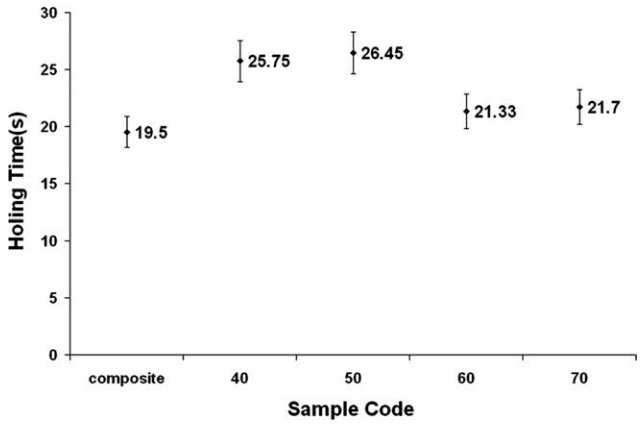

Figure 5. Pierced time of highly filled nanocomposites based on phenolic resin.

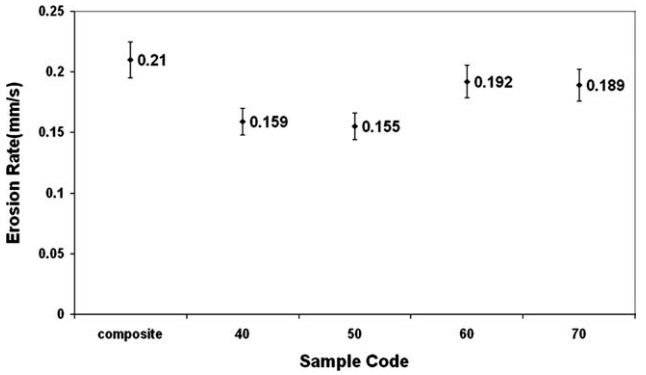

Figure 6. Erosion rates of highly filled nanocomposites based on phenolic resin.

nanocomposites, a combination of solution and in-situ intercalation methods was used. The preparation steps are summarized in Figure 2. All samples pre-cured at 100°C for 30 min, then cured at 160°C and 1 bar pressure for 1 h using vacuum bag molding method. Finally, the samples were postcured for 30 min at 160°C. The formulation of all samples is given in Table III.

The final samples were flat panels of 10 × 100 × 100 mm with a sandwich structure, formed from nanocomposite layer of 8 mm and aluminum layer of 2 mm as substrate, which used to determine the heat diffusion through the insulator thickness. Similar samples with dimensions of 4 × 100 × 100 mm were used for determining the erosion rate.

Characterization

The structure of the polymer-layered silicate nanocomposites has traditionally been elucidated by X-ray diffraction (XRD) and transmission electron microscopy (TEM) techniques.[29] To analyze prepared samples by XRD, a Miniflex diffractometer using Cu-K_α radiation with a dwell time of 1° min^{-1}, in the 2θ Bragg-Brentano geometry was used. Because TEM analysis requires substantial skills in specimen preparation, presence of asbestos cloth reinforcement in prepared samples eliminates the usefulness of TEM information. However, to evaluate the XRD results, TEM image was taken for organoclay/phenolic matrix nanocomposite in the absence of asbestos fibers.

The microstructure of a typical nanocomposite containing 50 phr organoclay was observed, using a TEM (EM 208 S, Philips) with an acceleration voltage of 100 kV. The sample was cut into 70–100 nm thick sections using a diamond knife and placed onto a 400 mesh copper grid.

A scanning electron microscope (CanScan FE microscope) equipped with a microanalyzer (EDAX) was used for imaging and elemental analysis. Thermogravimetric analysis (TGA) has been used to evaluate the performance of the ablative material and determine the kinetic parameters of thermal degradation process. Moreover, differential scanning calorimeter (DSC) has been used to calculate the heat of ablation and specific heat capacity of the samples. These tests were carried out by STA 409—NETZSCH instrument.

The thermal conductivity of laminate was measured at room temperature by using a comparative steady state method against a reference sample according to ASTM E1225-87. The method and formulation for calculation of thermal conductivity of samples through their thickness at transient condition of oxyacetylene flame test was reported in our previous works.[30,31]

The density and porosity of the composite laminate were determined at room temperature with submerging the sample in water according to ASTM D-4018. It is assumed that the density of the composite in thermal degradation condition depends on the mass fraction of polymer remaining in the solid, char, and porosity created during decomposition. The formulation for calculation of density of samples as a result of thermal degradation was mentioned in our previous article.[31]

Specific heat capacity measurements were performed with a differential scanning calorimeter (DSC 2000—NETZSCH) according to ASTM E-1265, at a heating rate of 10 K min^{-1} beneath the thermal degradation temperature of samples. The formulation for calculation of specific heat capacity of samples as a result of thermal degradation was also mentioned in the same reference.[31]

To evaluate the thermal behavior and ablation performance of the ablative insulators, the oxyacetylene flame test was performed according to ASTM E-285–80. This test can create hot gases with 3000 K and 8 × 10^6 W mK^{-1} heat flux. Hot combustion gases were directed perpendicularly to the specimen surface. The results of the test were used to elucidate the thermal behaviour of the ablative materials.

RESULTS AND DISCUSSION

Morphology

A TEM picture of 50 phr clay is shown in Figure 3. The TEM picture shows that an exfoliated morphology exists within the nanocomposite sample in the absence of asbestos fibers. Figure 4(a) shows the XRD pattern of montmorillonite, and Figure 4(b) shows those of nanocomposite and composite samples with no significant differences. It indicates primary silicate diffraction at about 2.7° for montmorillonite, corresponding to

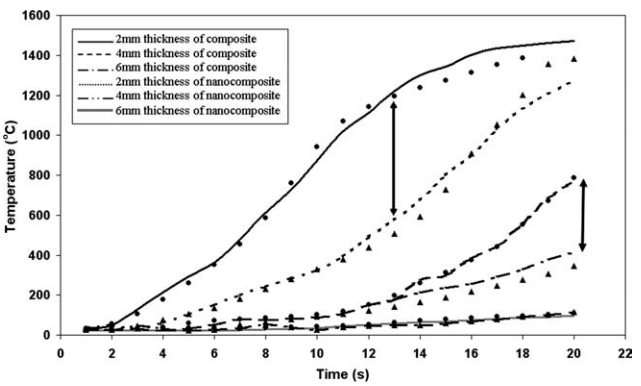

Figure 7. The experimental temperature distribution through the thickness of composite and nanocomposite containing 50 phr organoclay in the oxyacetylene flame test. Dot points and lines are experimental and theoretical results, respectively.

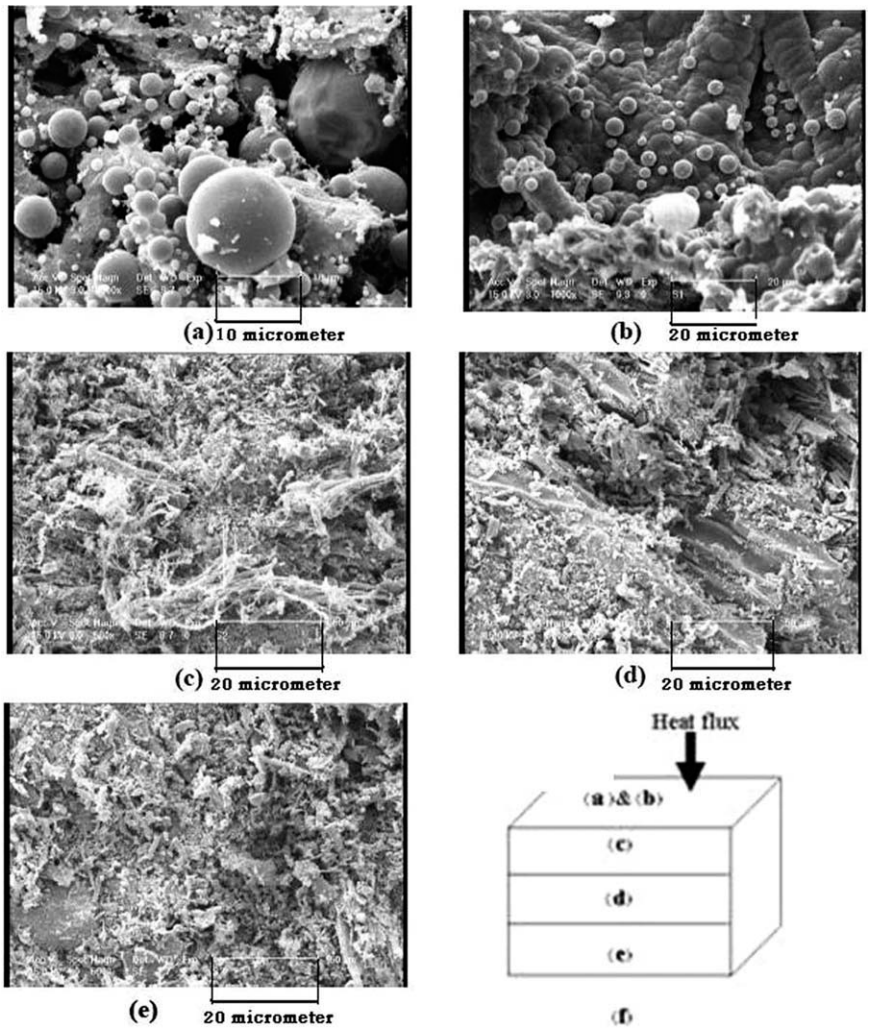

Figure 8. The scanning electron micrographs of ablative composite after oxyacetylene test: (a) and (b) top surface, (c), (d), and (e) lateral surfaces, and (f) illustrating of heat flux direction.

a d-spacing of about 31.5Å. The presence of these diffraction peaks implies the existence of the stacks of silicate layers with high degree of order. The absence of basal reflection in all nanocomposite patterns indicates the disruption of stacking order of the silicate layers, which implies that the exfoliated morphology was developed for nanocomposite samples.

Ablation Performance

Figure 5 shows pierced times of nanocomposites because of oxyacetylene flame test (at 3000 K hot gas temperature and 8×10^6 W m^{-2} heat flux). It indicates that pierced times for all nanocomposite samples are higher than that of the composite sample (at least 10% higher). Erosion rate of highly filled nanocomposites was illustrated in Figure 6. Lower erosion rate for nanocomposite samples means that they have higher ablation performance.

Nanocomposite containing 50 phr of organoclay shows the highest ablation performance (35% higher than that of composite counterpart). The decreasing of ablation performance of nanocomposites involving higher organoclay level than 50 phr is due to lack of adequate resin to wet the nanocomposite system and to bond its components together at pyrolysis conditions.

Determining the pierced time and erosion rate for ablative materials are appropriate criteria to evaluate the ablation performance of the insulator and the thermal diffusion depth through its surface under oxyacetylene test. This information is required for mathematical modeling of ablation behavior. Hence, in next sections, we focused mainly on the composite and nanocomposite containing 50 phr organoclay. Figure 7 indicates the temperature distribution through the thickness of highly filled nanocomposite containing 50 phr of organoclay and composite counterpart using the oxyacetylene flame test (3000 K hot gas temperature and 8×10^6 W m^{-2} external heat flux).

Oxyacetylene test time interval and heat flux have been chosen in a way that the first thermocouple (2 mm from top surface) is sat in char zone, the second thermocouple (4 mm from top surface) is sat in pyrolysis zone, and the third thermocouple

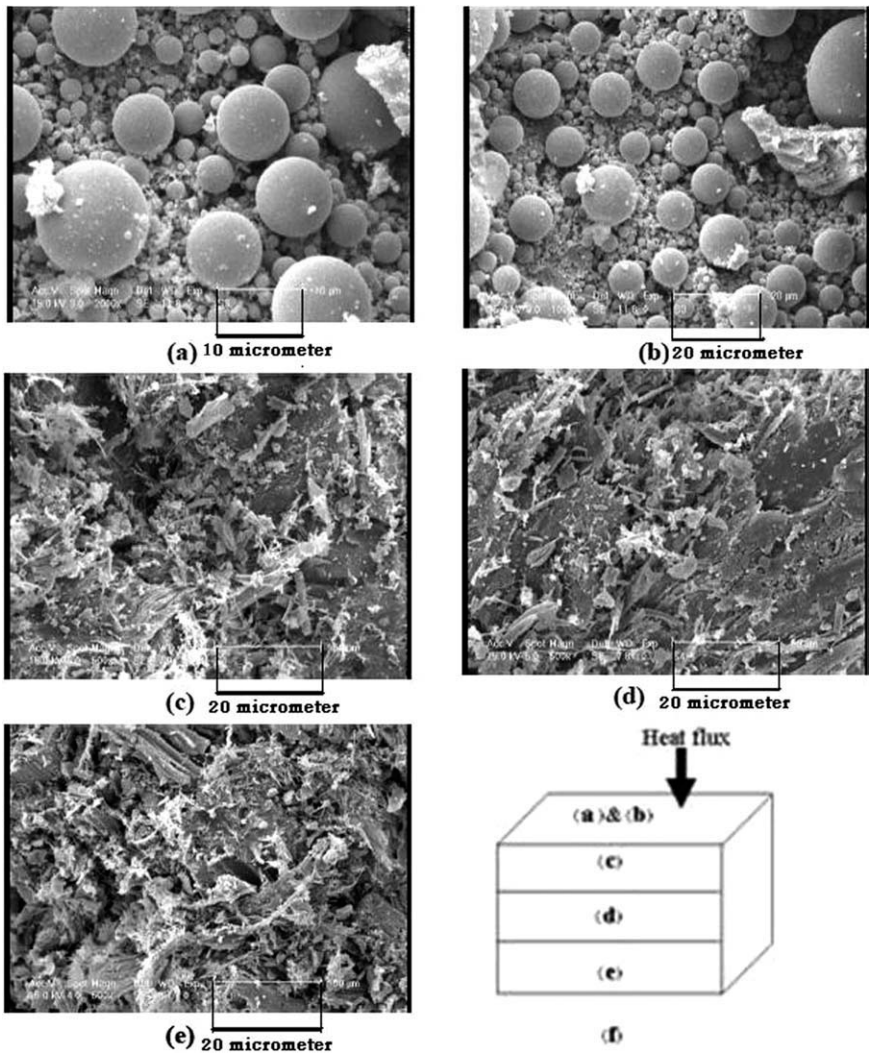

Figure 9. The scanning electron micrographs of ablative nanocomposite containing 50 phr organoclay after oxyacetylene test: (a) and (b) top surface, (c), (d), and (e) lateral surfaces, and (f) illustrating of heat flux direction.

(6 mm from top surface) is sat in virgin zone. Figure 7 also shows that the following points:

(a) In the first (char) zone, value of back temperature for nanocomposite sample is lower than that of composite sample. As known, the lower value of back temperature is one of the key factors to indicate the higher insulation performance of nanocomposite sample compared with its composite counterpart. As it is observed at about half oxyacetylene test time interval, the insulation performance of nanocomposite, containing 50 phr of organoclay, reaches near 5 times of that of its composite counterpart (about 250%). Insignificant difference between the results of composite sample and highly filled nanocomposite sample in remaining time interval is due to incomplete formation of char layer at the beginning of the test and splitting of char layer at the end of test. In general, prominent difference between the ablation behavior of composite and highly filled nanocomposite samples in char zone, depends clearly on the nature of this zone in these cases.

(b) In the second (pyrolysis) zone, higher insulation performance of highly filled nanocomposite is clearly observable, too. In the beginning of oxyacetylene test, there is no significant difference between the temperatures of the samples, but after a while, almost at half of the test interval time, difference between pyrolysis temperatures of composite and nanocomposite samples becomes significant and reaches to nearly twice value (about 200%). In fact when char layer is formed in pyrolysis zone, highly filled nanocomposite sample shows opposite behavior with respect to composite sample. When the char layer formation starts in second zone, this difference becomes prominent. This behavior confirms the key role of ceramic char layer on ablation performance of highly filled nanocomposite sample. Formation of char layer on surface of sample makes the performance

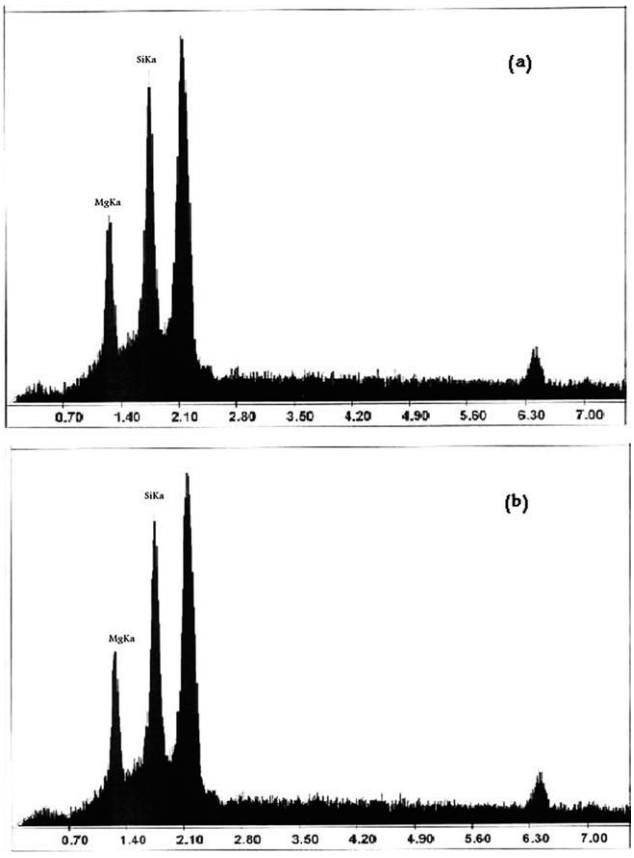

Figure 10. Elemental analysis of the surfaces of (a) composite sample and (b) nanocomposite sample containing 50 phr organoclay after oxyacetylene test.

of highly filled nanocomposite sample elevated to 150% compared with that of low-filled nanocomposites.[4,22,30]

(c) In the third (virgin) zone, which remains intact during oxyacetylene test time interval, there is no sensible difference between the performances of nanocomposite and composite samples. In fact, existence of layered silicates in polymeric matrix exhibits opposite effects when the ablation initiates. On pyrolysis, the layered silicates form a uniform ceramic char layer, as a preventive factor against heat diffusion, which may lead to significantly higher resistance to oxidation and mechanical erosion.[4,22] However, organoclay containing materials start to decompose earlier than neat polymer.[24] Furthermore, higher loading of organoclay results in heat capacity reduction of nanocomposite. These two factors promote the heat diffusion. In char and pyrolysis zones, the first factor is dominant, but in virgin zone, by increasing the thickness of the sample, neither factor is dominant and possesses almost the same effects.

In other words, the most differences between ablation performance of composite and nanocomposite samples are the consequence of thermal degradation, char formation, and nature of the ceramic char layer. Figures 8 and 9 show SEM micrographs of the asbestos-phenolic composite and nanocomposite (containing 50 phr organoclay) samples after oxyacetylene flame test, respectively. These figures show top surface (surface of char zone), lateral surfaces, and heat flux direction. The characteristics of various regions, i.e., virgin zone, porous pyrolysis zone, and char zone, are shown in these figures.

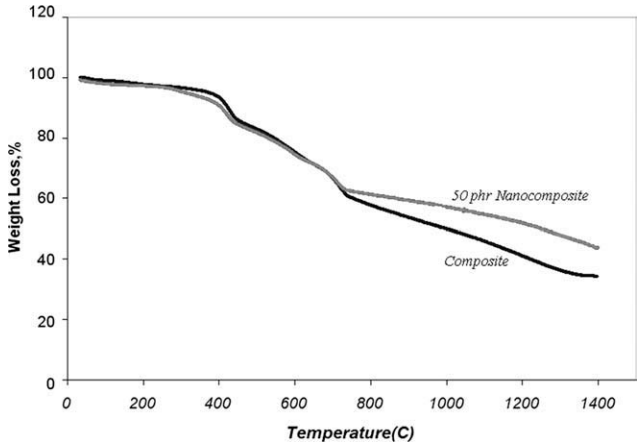

Figure 11. TGA plots of composite and highly filled nanocomposite sample under air atmosphere.

In char zone, nanoscopic porous morphologies are also observed. The melted combustion products formed particles with spherical shape. Comparison of Figures 8 and 9 (a,b) clearly shows that the char formed on the surface of composite sample has higher porosity than that formed on the surface of nanocomposite sample. However, on the surface of nanocomposite sample formed a uniform and regular char compared with composite sample.

Figure 10 shows the elemental analysis results (EDAX) of the char layers on composite and nanocomposite (containing 50 phr organoclay) samples after oxyacetylene flame test. Figure 10(a) indicates that the existence of silicon and magnesia in the char of the composite sample, whereas Figure 10(b) shows the existence of silicon, magnesia (at very higher ratio of Si/Mg), aluminum, and sodium in the char of the nanocomposite sample.

Table IV. The Kinetic Parameters of the Samples at the First and Second Half Zones

Kinetic parameters of the samples	E (J mol^{-1})	$E_g - E_c$ (J mol^{-1})	A_g/A_c	n
Composite (at the first half zone)	2.3×10^7	3.16×10^7	21.39	1.8
Nanocomposite (50 phr of organoclay) (at the first half zone)	2.45×10^7	2.6×10^7	12.36	2.1
Composite (at the second half zone)	4.07×10^7	2.43×10^7	10.61	0.8
Nanocomposite (50 phr of organoclay) (at the second half zone)	3.84×10^7	1.53×10^7	3.37	0.6

Applied Polymer SCIENCE

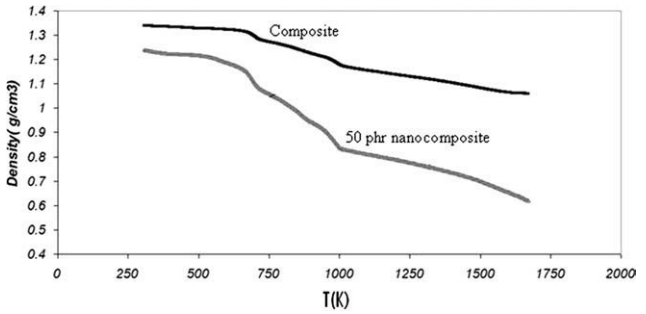

Figure 12. The variation of density versus temperature of the nanocomposite in comparison with composite.

After oxyacetylene flame test, such analysis demonstrates that the mineral composition of composite sample changes from clinochrysotile [$Mg_3Si_2O_5(OH)_4$] to forsterite (Mg_2SiO_4), whereas the mineral composition of nanocomposite sample contains forsterite (Mg_2SiO_4) and sodium aluminum silicate ($NaAlSiO_4$). Therefore, it can be concluded that the char layer of ablative nanocomposite sample contains the ceramic-based aluminum silicate, which was reported in our previous works, as well.[22,30]

Thermal Degradation Kinetics

TGA thermograms for composite and nanocomposite samples containing 50 phr are shown in Figure 11. In general, major weight losses are observed on the range of ~ 400–700°C for all the specimens. Evidently, the temperature range of thermal decomposition of the nanocomposite sample shifts to right in comparison with that of the composite sample, which implies that nanocomposite sample has higher thermal stability. At the temperatures higher than ~ 800°C, mainly the inorganic residue remained. The residual masses of composite and nanocomposite sample containing 50 phr of organoclay at 1400°C are 34 wt % and 44 wt %, respectively.

Generally, for conventional low-filled nanocomposite, it is reported that the presence of organoclay in polymeric matrix enhances its thermal stability. This is attributed to the improved barrier properties of nanocomposites that hinder the diffusion out of the material.[22,24,30] As known, to enhance the compatibility of layered silicates with polymers for achieving appropriate dispersion, layered silicates are usually modified with organic surfactants, e.g., alkyl ammonium. It should be noted that some

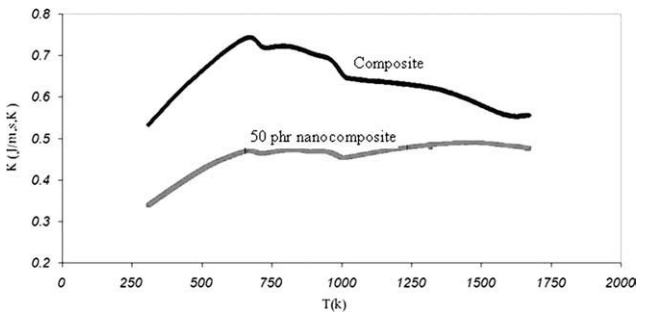

Figure 13. Nonmonotonic variation of heat conductivity of nanocomposite in comparison with composite.

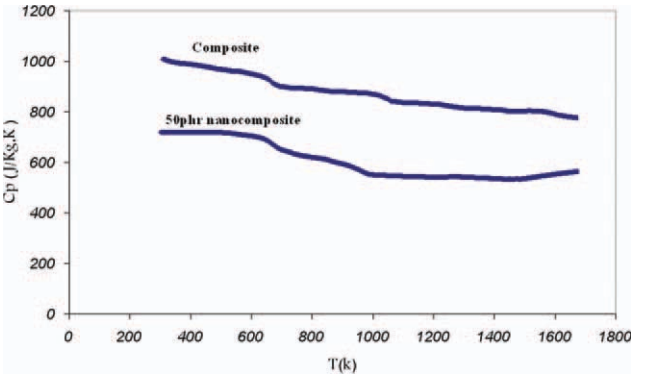

Figure 14. The change of specific heat of the nanocomposite in comparison with the composite under heating. [Color figure can be viewed in the online issue, which is available at wileyonlinelibrary.com.]

of the organic surfactant may not be ionically bound and only adsorbed onto the surface of layered silicates. Alkyl ammonium is thermally unstable and decomposes around 200°C. Thus, the presence of such a large amount of low molecular weight surfactant may adversely affect the thermal stability of highly filled nanocomposites. It is also important to note that dehydroxylation of aluminosilicate also occurs in the range of 500–700°C. Accordingly in low-filled nanocomposites, the barrier property is prominent, whereas in highly filled nanocomposites, the negative effect of thermal decomposition of alkyl ammonium salts in the clay galleries are dominant. These factors are the major reasons for poor thermal stability of highly filled nanocomposites.[24]

As mentioned before, the scope of this section is to determine the kinetic parameters of the thermal degradation of samples by TGA. The knowledge of these parameters is required to calculate the variation of thermophysical properties and usage of ablation equations. The steps of the thermal degradation of a polymer in composite have been described elsewhere.[21,22] In this work, we used those results as well. The thermal degradation kinetic parameters for all samples are given in Table IV.

Thermophysical Properties

Figure 12 shows the comparative density variation of the nanocomposite and composite samples versus temperature. As it is observed, the initial density and also the final density of nanocomposite sample are lower than its composite counterpart. This is due to the porosities created in char layer of specimens during thermal degradation. The presence of surface modifier in organoclay is the main reason.

Figure 13 indicates nonmonotonic character of varying heat conductivity of the nanocomposite sample in comparison with composite sample. Increase in the heat conductivity coefficient at the initial stage of heating is related to the increase of heat conductivity of the polymer phase. On further heating of the specimens to the temperature where pyrolysis begins, the heat conductivity coefficient decreases. This is attributed to the formation of further pores in the samples. At the end of pyrolysis and char formation, heat conductivity coefficient grows again

due to increase in the heat conductivity coefficient of the hot char.

In Figure 13 several points are remarkable:

a. Generally, heat conductivity of highly filled nanocomposite sample is lower than that of the composite sample. It is due to the difference in components, nature of composite, and nanocomposite samples. In fact, highly filled nanocomposite sample containing surface modified layered silicates exhibits lower conductivity than the phenolic resin itself.
b. During heating, the heat conductivity variation of highly filled nanocomposite sample is lower than that of the composite sample. It is due to barrier effect of silicate layers against heat diffusion through bulk.
c. The final values of heat conductivity of nanocomposite sample are lower than that of the composite samples. It is because of ceramic char formation on the surface of nanocomposite sample that prevents heat diffusion.

Figure 14 shows the change of specific heat of the nanocomposite sample in comparison with composite under heating. The specific heat of each sample was determined as the average value of the specific heat of its components. When the thermal degradation and pyrolysis of polymer matrix begins, the volume fraction of every components of composite changes and makes the specific heat to change. As it is expected, the specific heat capacities of nanocomposite samples are generally lower than that of the composite samples.

Ablation Modeling

Figure 7 also shows the temperature distribution through the thickness of composite and nanocomposite (containing 50 phr organoclay) samples under oxyacetylene flame test. In this figure, dot points and lines are experimental and theoretical results, respectively. A good agreement between the numerical and experimental results is observed for all specimens (negligible differences between experimental and theoretical values are due to the abandon effect of fluid stream force of oxyacetylene flame in the calculation of the surface erosion).

Consequently, this model is able to predict the performance of ablative materials with moving boundary for ablator surface and to solve nonlinear conservation equations of energy, mass, and decomposition at unsteady state condition. It is completely reliable for prediction of charring and ablating materials to severe aerothermal/erosive environments with moving surface and change phase by changing density, conductivity, and heat capacity.

CONCLUSIONS

The polymer-layered silicate nanocomposites result in improvement in ablative performance relative to the polymeric composite. With nanoclay, a relatively tough inorganic ceramic layer was formed during ablation of the nanocomposites. This refractory ceramic creates the secondary heat shield to protect the initial heat shield system. According to the nanocomposite heat shield ablation mechanism that is presented in this work, the main results of thermal stability and ablation performance are given as follow:

1. Ablation performance of highly filled nanocomposites is very higher than their composite counterpart. Nanocomposite sample containing 50 phr of organoclay has an erosion rate of 135% lower than that of the composite sample.
2. The main reason of higher performance of highly filled nanocomposites is the formation of ceramic char layer on the ablator surface. The main component of this ceramic layer is sodium aluminum silicate which protects the ablation char layer against the thermal erosion effects. Char layer formation, which was previously reported for low filled nanocomposites, exhibits more efficiently in the case of highly filled nanocomposites.
3. Two opposite effects on thermal stability can be observed in the polymeric organoclay nanocomposites: in one hand, the presence of layered silicate that has low heat capacity and loss of alkyl ammonium surfactant decreases the thermal stability of sample, and on the other hand, fine dispersion of organoclay has a barrier effect that increases thermal stability of nanocomposite. Therefore, no significant difference is observed between thermal stability of highly filled nanocomposite and its composite counterpart.
4. Mathematical model is adequately confirmed by the experimental data of the thermophysical and ablation properties of nanocomposites. The mathematical model propounds a simple tool, which allows ablation process simulation for designing of the optimal thickness of a nanocomposite heat shield.
5. Bearing in mind that albeit asbestos fibers have unique thermal properties for this especial application, they are banned in many countries around the world for their severe implications in human health.

ACKNOWLEDGMENTS

The authors would like to thank Tarbiat Modares University and Iran Nanotechnology Initiative Council (INIC) for financial support of this work.

REFERENCES

1. Lin, W. S. *Int. J. Heat Mass Transfer* **2005,** *48*, 5504.
2. Firouzmanesh, M. R.; Aref Azar, A. *J. Appl. Polym. Sci.* **2003,** *88*, 2455.
3. Kanevce, L. D.; Kanevece, G. H. Third International Conference on Inverse Problems in Engineering, Port Ludlow, WA, **1999.**
4. Vaia, R. A.; Price, G.; Ruth, P. N.; Nguyen, H. T.; Lichtenhan, J. *Appl. Clay. Sci.* **1999,** *15*, 67.
5. Torre, L.; Kenny, J. M.; Maffezzoli, A. M. *J. Mater. Sci.* **1998,** *33*, 3137.
6. Bradford, J. E.; Olds, J. R. 24nd AIAA/ASME/ASE/ASEE Propulsion Conference & Exhibit, Sacramento, CA, **2006.**
7. Alelio, G. F. D.; Parker, J. A. Ablative Plastics; Marcel Dekker Inc.: New York, **1971.**

8. Ogasawara, T.; Ishikawa, T. *J. Am. Ceram. Soc.* **2001,** *84*, 1559.
9. Siddiqui, A. O.; Balasubrahmanyam, G. *J. Reinf. Plast. Compos.* **2005,** *24*, 993.
10. Dimitrienko, Y. I.; Efremov, G. A.; Chernyavsky, S. A.; Medvedev, Y. V. *Appl. Compos. Mater.* **1996,** *2*, 367.
11. Severov, A. A.; Gracheva, L. I.; Koloskova, V. N.; Vengzhen, V. *Strength Mater.* **1992,** *24*, 327.
12. Gibson, A. C.; Hume, J. *Plas. Rubber. Compos. Process. Appl.* **1995,** *23*, 175.
13. Florence, D. E.; Hiltz, A. A.; Lowe, D. L. *J. Spacecraft Rockets* **1986,** *5*, 1278.
14. Chen, Y. K.; Milos, F. S. *AIAA J.* **1994,** *98*, 475.
15. Torre, L.; Kenny, J. M. *J. Mater. Sci.* **2000,** *35*, 4563.
16. Park, J. K.; Cho, D.; Kang, T. J. *Carbon* **2004,** *42*, 795.
17. Cho, D.; Lee, J. K.; Yoon, B. I. *J. Mater. Sci. Lett.* **1993,** *12*, 1894.
18. Sreejith, P. S.; Krishnamurthy, R.; Malhotra, S. K. *J. Mater. Process Technol.* **2007,** *183*, 88.
19. Koo, J. H.; Stretz, H.; Bray, A.; Weispfenning, J.; Luo, Z. P.; Blanski, R.; Ruth, P. 44th AIAA/ASME/ASCE/AHS Structures, Structural Dynamics, and Materials Conference, Norfolk, VA, **2003.**
20. Koo, J. H.; Stretz, H.; Weispfenning, J. T.; Luo, Z.; Wootan, W. 45th AIAA/ASME/ASCE/AHS/ASC Structures, Structural Dynamics & Materials Conference, Palm Springs, CA, **2004.**
21. Bahramian, A. R.; Kokabi, M.; Famili, M. H. N.; Beheshty, M. H. *Iran Polym. J.* **2007,** *16*, 375.
22. Bahramian, A. R.; Kokabi, M.; Beheshty, M. H.; Famili, M. H. N. *J. Hazard Mater.* **2008,** *150*, 136.
23. Natali, M.; Kenny, J.; Torre, L. *Compos. Sci. Technol.* **2010,** *70*, 571.
24. Dasari, A.; Yu, Z. Z.; Mai, Y. W. *Nanotechnology* **2007,** *18*, 1.
25. Liu, Y.; Zhu, M.; Liu, X. *Polymer* **2006,** *47*, 1.
26. Salahuddin, N.; Moet, A. *Eur. Polym. J.* **2002,** *38*, 1477.
27. Lu, Y. L.; Li, Z.; Yu, Z. Z. *Compos. Sci. Technol.* **2007,** *67*, 2903.
28. Wu, T.; Xie, T.; Yang, G. *J. Polym. Sci. Part B: Polym. Phys.* **2008,** *46*, 2335.
29. Sheng, N.; Boyce, M. C.; Parks, D. M.; Rutledge, G. C.; Abes, J. I.; Cohen, R. E. *Polymer* **2004,** *45*, 487.
30. Bahramian, A. R.; Kokabi, M.; Beheshty, M. H.; Famili, M. H. N. *J. Hazard. Mater.* **2009,** *166*, 445.
31. Bahramian, A. R.; Kokabi, M.; Famili, M. H. N.; Beheshty, M. H. *Polymer* **2006,** *47*, 3661.